

Nanoscale Advances

Accepted Manuscript

This article can be cited before page numbers have been issued, to do this please use: Y. Cohen, G. Cohen, D. Tworowski, N. Eretz-Kdosha, E. Silberstein, E. Fallik and E. Poverenov, *Nanoscale Adv.*, 2022, DOI: 10.1039/D2NA00005A.



This is an Accepted Manuscript, which has been through the Royal Society of Chemistry peer review process and has been accepted for publication.

Accepted Manuscripts are published online shortly after acceptance, before technical editing, formatting and proof reading. Using this free service, authors can make their results available to the community, in citable form, before we publish the edited article. We will replace this Accepted Manuscript with the edited and formatted Advance Article as soon as it is available.

You can find more information about Accepted Manuscripts in the [Information for Authors](#).

Please note that technical editing may introduce minor changes to the text and/or graphics, which may alter content. The journal's standard [Terms & Conditions](#) and the [Ethical guidelines](#) still apply. In no event shall the Royal Society of Chemistry be held responsible for any errors or omissions in this Accepted Manuscript or any consequences arising from the use of any information it contains.

ARTICLE

Received 00th January 20xx,
Accepted 00th January 20xx

DOI: 10.1039/x0xx00000x

Biocompatible nanocarriers for passive transdermal delivery of insulin based on self-adjusting *N*-alkylamidated carboxymethyl cellulose polysaccharidesYael Cohen,^{b,a} Guy Cohen,^{c,d} Dmitry Tworowski,^e Noy Eretz-Kdosha,^c Eldad Silberstein,^f Elazar Fallik,^a and Elena Poverenov^{*a}

In this work, we present biocompatible nanocarriers based on modified polysaccharides capable of transporting insulin macromolecule through human skin without any auxiliary techniques. *N*-alkylamidated carboxymethyl cellulose (CMC) derivatives, CMC-6 and CMC-12, were synthesized and characterized using attenuated total reflectance fourier transform infrared (ATR-FTIR) and nuclear magnetic resonance (NMR) spectroscopy, gel permeation chromatography and thermogravimetric, calorimetric and microscopic techniques. The prepared modified polysaccharides spontaneously assemble into soft nanoaggregates capable of adjusting to both aqueous and lipid environments. Due to this remarkable self-adjustment ability, CMC-6 and CMC-12 were examined for transdermal delivery of insulin. First, a significant increase in the amount of insulin present in lipid media upon encapsulation in CMC-12 was observed *in vitro*. Then, *ex vivo* studies on human skin were conducted. Those studies revealed that the CMC-12 carrier led to enhancement of transdermal insulin delivery, showing a remarkable 85% insulin permeation. Finally, toxicity studies revealed no alteration in epidermal viability upon treatment and the absence of any skin irritation or amplified cytokine release, verifying the safety of the prepared carriers. Three-dimensional (3D) molecular modeling and conformational dynamics of CMC-6 and CMC-12 polymer chains explained their binding capacities and the ability to transport insulin macromolecule. The presented carriers have the potential to become a biocompatible safe and feasible platform for the design of effective systems for transdermal delivery of bioactive macromolecules in medicine and cosmetics. In addition, transdermal insulin delivery reduce pain and infection risk in comparison to injections that may increase the compliance and glycemic control of diabetic patients.

Introduction

Transdermal delivery of therapeutic agents is a very promising field in modern medicine. However, it is challenging because of strong lipid skin barrier. To facilitate transdermal penetration of active molecules, especially hydrophilic ones, delivery systems must be developed.¹

Biopolymer-based delivery systems are widely studied and utilized in numerous fields such as medicine, tissue engineering, cosmetics and food science.^{2–6} Among all biopolymers, polysaccharides represent favourable candidates for the construction of biocompatible delivery systems since they are

^a Agro-Nanotechnology and Advanced Materials Center, Institute of Postharvest and Food Sciences, Agricultural Research Organization, The Volcani Center, Rishon LeZion 7505101, Israel.

^b Institute of Biochemistry, Food Science and Nutrition, Faculty of Agriculture, Food and Environment, The Hebrew University of Jerusalem, Rehovot 76100, Israel.

^c The Skin Research Institute, Dead Sea & Arava Science Center, Masada 86910, Israel

^d Eilat Campus, Ben-Gurion University of the Negev, Eilat 8855630, Israel

^e Department of Structural Biology, Weizmann Institute of Science, 76100 Rehovot, Israel.

^f Department of Plastic Surgery, Soroka University Medical Center, Ben-Gurion University of the Negev, Beer-Sheva, Israel.

* Corresponding author: E-mail: elenap@volcani.agri.gov.il. Phone: 972-39683354.

† Electronic Supplementary Information (ESI) available: comprehensive TGA data derivatives, calibration curve of methylene blue and immunoassay method validation analysis. See DOI: 10.1039/x0xx00000x



hypoallergenic, non-toxic, biodegradable and widely available.^{7–9} In addition, polysaccharides also possess the significant advantage of a defined monomer structure that allows their rational modification and the precise tuning of their properties.^{10–12} Numerous delivery systems, including polysaccharide-based systems, have been investigated for transdermal applications and demonstrated notable success in the delivery of small molecules.^{1,13–17}

However, transdermal delivery of high molecular-weight molecules, remains challenging. The molecules with molecular weight (MW) of higher than 500 Da are usually injected.¹⁸ For instance, insulin is an eminent example of a macromolecule for which transdermal delivery could significantly improve the quality of life of numerous patients.^{19,20} The hormone insulin is a daily treatment for patients suffering from diabetes mellitus, a metabolic disorder that causes abnormal accumulation of glucose in the blood.²¹ As a hydrophilic macromolecule that is 5.5–6.0 kDa in size, insulin can barely pass dermal barriers. Therefore, millions of patients must inject insulin at least once per day or more, or use subcutaneous insulin devices. These options are unpleasant, require strict self-discipline and involve risks of microbial infection, local tissue necrosis and nerve damage.¹⁹ In addition, using non-invasive transdermal delivery of insulin is less painful than hypodermic injections and can also be used by patients with needle phobia. Transdermal delivery is also pharmacokinetically preferable to other non-invasive methods such as oral administration due to the lack of first-pass effect of insulin. Collectively, these benefits can increase patients compliance and glycaemic control.^{19–21}

Advanced physical methods to help transport bioactive macromolecules, including insulin, across the skin barrier have been reported. These methods include the use of microneedles,^{22–26} ultrasound-mediated penetration,^{26,27} transdermal photopolymerization²⁸ and skin electroporation.^{29,30} Delivery methods enabling the transport of insulin without the auxiliary, physical penetration techniques, are more feasible. Therefore, molecular systems for passive transdermal delivery have recently attracted a great deal of attention. To date, only a few examples of such vehicles have been reported; those systems have been based on synthetic peptides, phospholipids and polysaccharides.^{31–35} Coadministration with synthetic peptides,³¹ CaCO₃ based nanoparticles poly(ester amide) based hybrid hydrogels³⁶ or choline ionic liquid³⁷ and solid in oil nanodispersion³⁸ are examples of advanced approaches that have been used to facilitate the transport of insulin. Nanoparticles containing insulin had been also shown to enhance insulin permeation. For instance, Zhao *et al.* demonstrated that supercritical antisolvent (SAS) micronization process can produce nanoparticle with high permeation rate that was linear for 6 hr.³⁹ Gold nanoparticles⁴⁰ as well as nanorods with near infrared light irradiation⁴¹ had been found active *in vivo*. To the best of our knowledge, no polysaccharide-based systems for transdermal delivery of insulin have been previously reported.

Here, we report the synthesis of polysaccharidebased carriers capable of adjusting their structure to various environments and consequently facilitating cross-phase

transport. The prepared systems were used for passive transdermal delivery of insulin. Skin toxicity studies were also performed, to verify the efficacy and safety of the prepared materials.

Experimental section

Materials

Sodium carboxymethyl cellulose (MW = 250 kDa; DS = 0.9), *n*-dodecylamine and *N*-hydroxysuccinimide (NHS) were purchased from Acros Organics (Geel, Belgium). *n*-Hexylamine pyrene, insulin (monomer, human recombinant) and insulin labeled with fluorescein isothiocyanate (FITC; human recombinant) were purchased from Sigma Aldrich (Steinheim, Germany). 1-(3-Dimethylaminopropyl)-3-ethylcarbodiimide hydrochloride (EDC) was purchased from Alfa Aesar (Lancashire, UK). Dextran standards were purchased from PSS Polymer (Mainz, Germany). Ethanol and ethanol absolute were purchased from Gadot Group (Netanya, Israel). Water, high performance liquid chromatography (HPLC) grade, was purchased from Bio Lab (Jerusalem, Israel). Organic cold pressed sunflower oil (SO) was purchased from Joe & Co. (Vicenza, Italy). Deionized water (DI) was obtained by mechanically filtering water through a Treion TS1173 column. Deuterated solvent for the NMR analysis (D₂O) was purchased from Armar Chemicals (Döttingen, Switzerland). All reagents and solvents were used without any further purification.

Methods

Synthesis of CMC-6 and CMC-12. *N*-alkylamidated modifications were prepared by dissolving 0.58% (w/w) carboxymethyl cellulose (CMC) in 100 mL DI at 60 °C. Once the solution achieved homogeneity, it was cooled down to room temperature and 1.3 mmol of EDC and 1.3 mmol of NHS were added. After 2.5 h of stirring, 1.3 mmol of a selected amine (hexyl amine or dodecyl amine) were added and the solution was stirred overnight (dodecylamine was first dissolved in 15 mL of absolute ethanol and then added to the reaction solution at 40 °C). According to the manufacturer, the commercial CMC's DS is 0.9, so amount of carboxymethyl groups [mole] available for *N*-alkylamidation was calculated as [(0.58 g / 270 g/mol) * 0.9], where 0.58 g is the mass of the CMC polymer, 270 is the MW of the CMC monomer and 0.9 is the monomer molar fraction. Amines, EDC and NHS were added at 0.7 eq in respect to CMC's carboxymethyl groups. The *N*-alkylamidated derivatives CMC-6 and CMC-12 were precipitated by adding six times the volume of ethanol (vs. the reaction solution volume), isolating the material *via* centrifugation, washing it with ethanol three times, and then drying it in a vacuum desiccator overnight.

Characterization of CMC-6 and CMC-12

Attenuated total reflection-Fourier transform infrared (ATR-FTIR) spectroscopy. ATR-FTIR spectroscopy was performed using a Thermo Scientific Nicolet iS5 FTIR spectrometer (USA), equipped with diamond ATR (thermo scientific Everest ATR), fast recovery deuterated triglycine sulfate detector, KBr/Ge midinfrared optimized laser beam splitter, solid state near-IR diode laser temperature controlled and Mid-infrared Ever-Glo



source type. Calibration was done using air sample and modified CMC powders were subjected to 32 scans at a 0.5 cm⁻¹ resolution between 500 and 4000 cm⁻¹.

Nuclear magnetic resonance (NMR). ¹H NMR spectra were recorded using Bruker Avance I and Avance III NMR 400 MHz spectrometers (USA). Chemical shifts are reported in parts per million (ppm). ¹H-NMR spectra were calibrated to the solvent residual peak (H₂O at 4.79 ppm). All of the NMR samples were prepared using D₂O as a solvent at 298K.

Degree of substitution. The total organic carbon (TOC) and the total nitrogen (TN) contents of CMC, CMC-6 and CMC-12 were determined in water by high temperature catalytic combustion and chemiluminescence detection using a Shimadzu (USA) ASTM D 8083 analyzer elemental analyzer (USA, TOC-L with TNM). CMC, CMC-6 and CMC-12 powders were dissolved in distilled water to a final concentration of 0.2 mg/mL. The percentage of CMC substitution by hexyl / dodecyl amide was calculated using the following equation:

$$\% \text{ substitution} = 100 * [\text{TN}(\text{CMC6 or CMC12})/\text{Mw}(\text{N})] / [\text{TOC}(\text{CMC})/\text{Mw}(\text{C})]$$

Gel permeation chromatography (GPC). The molecular weights and polydispersity indices of CMC, CMC-6 and CMC-12 were determined using gel permeation chromatography (GPC). Waters' Alliance system e2695 separations module was used (Waters, USA), equipped with a refractive index detector, model Blue 2414. The mobile phase was HPLC-grade water under isocratic elution for 30 min at a flow rate of 0.7 mL/min. The injection volume was 20 μL and the temperature of both the detector and the columns was 30 °C. Analyses were carried out using an ultrahydrogel column: 1000 Å, 12 μm, 7.8 mm × 300 mm, 2-4,000 kDa (Waters, USA). The molecular weights were determined according to a dextran standards kit with a number average molecular weight [M_n] range of 3,300-333,000 Da (PSS Polymer Standards Service GmbH, Germany). All data provided by the GPC system were collected and analyzed with the Empower 3 personal dissolution software. CMC, CMC-6 and CMC-12 powders were dissolved in the mobile phase to a final concentration of 1 mg/mL. The solutions were filtered through a 0.22 μm nylon syringe filter.

Thermogravimetric analysis (TGA). Thermogravimetric analysis (TGA) was performed using a Perkin-Elmer TGA 8000 device (TA Instruments, USA). Ceramic crucibles were loaded with 1–3 mg of each sample and heated from 50 °C to 800 °C at a rate of 10 °C/min under the flow of a N₂ atmosphere (20 mL/min).

Differential scanning calorimetry (DSC). Differential scanning calorimetry (DSC) measurements were conducted with a Perkin-Elmer DSC 6000 instrument (USA) calibrated using indium and zinc standards. Thermograms of each sample were obtained from the second heating run up to 440 °C, after the first run of heating up to 160 °C and cooling to 50 °C at a constant rate of 20 °C/min, under a N₂ purge of 20 mL/min. Aluminum crucibles with pierced lids were loaded with 5–15 mg of each sample.

Critical aggregation concentration (CAC) measurements. The critical aggregation concentrations of CMC-6 and CMC-12 were studied using the pyrene fluorescent probe method.⁴² The ratio between two specific peaks (*i.e.*, I₃ ~383 nm and I₁ ~373 nm) in

pyrene's spectrum was used as a quantitative measurement for the aggregation point. The diluent was prepared by adding 25 μL of the pyrene stock solution (0.49 mg/mL) to 50 mL of distilled water to give a final concentration of 1.2 μM. A 15 mg/mL CMC-6 solution or 1.5 mg/mL CMC-12 solution was dissolved in the diluent and the mixture was stirred overnight. Then, the prepared solutions were repeatedly diluted by a factor of 2 with the abovementioned diluent. 150 μL of each solution were loaded onto a 96-well plate. The fluorescence emission intensity was scanned for each well using a SynergyHTX multimode reader device (BioTek Instruments, USA). The excitation wavelength for pyrene is 340 nm and the emission band was recorded at 360–400 nm, with a resolution of 1 nm. All samples measured were kept at 26±1 °C. All measurements were done in triplicate. Critical aggregation concentration values were calculated as the intersection between two linear lines depicting aggregate formation dependent on concentration in solution.⁴²

Transmission electron microscopy (TEM). Samples (3 μL drop) of aqueous solutions of CMC-6 and CMC-12 (CMC-6: 20 mg/mL; CMC-12: 1.5 mg/mL) were placed on glow discharged TEM grids (ultrathin carbon on carbon lacey support film, 400 mesh copper grids, Ted Pella, Inc.). The excess liquid was blotted with filter paper and the grids were allowed to dry in the air. The samples were examined by a FEI Tecnai 12 G2 TWIN TEM operated at 120 kV. Images were recorded using 4k × 4k FEI Eagle CCD camera (ThermoFisher Scientific, USA).

Solubilization of CMCs in sunflower oil (a lipophilic medium). Aqueous CMC, CMC-6 and CMC-12 solutions (0.5 mL each) at a concentration of 25 mg/mL were added to 10 mL of sunflower oil. The resulting solutions were then heated to 100 °C with stirring, to evaporate any water and to yield a final polymer concentration of 1.25 mg/mL of the oil.

In vitro examination of the abilities of CMC-6 and CMC-12 to introduce insulin into a lipid environment

Encapsulation studies involving a spectrofluorometer. Labeled insulin (insulin-FITC) was added to the sunflower oil solutions of the CMC derivatives prepared as described above to reach an insulin-FITC concentration of 1 mg/mL and stirred at 23 °C for 48 h, while they were kept covered with aluminum foil. The prepared solutions were kept for a week at ambient temperature covered by aluminum foil for gravitational filtration. Then, 100 μL of each solution were loaded onto a 96 well plate. The fluorescence emission intensity was scanned for each well using a Synergyneo2 multimode reader device (BioTek Instruments, USA). The excitation wavelength for FITC was 490 nm and the emission band recorded was 510–700 nm, at increments of 5 nm. The fluorescent emission of insulin-FITC added to sunflower oil that did not contain any CMC was used as a control.

Encapsulation studies – confocal laser scanning microscopy (CLSM). Labeled insulin (insulin-FITC) was added to the sunflower oil solutions of the CMC derivatives prepared as described above to reach an insulin-FITC concentration of 0.5 mg/mL. The mixtures were stirred for 48 h, while they were kept covered by aluminum foil. The prepared solutions were kept for a week at ambient temperature, covered by aluminum foil, for



gravitational filtration. About 20 μL of each solution were loaded onto microscope slide. Images were acquired using a Leica SP8 laser scanning microscope (Leica, Wetzlar, Germany), equipped with an OPAL 488 nm laser, HC PL APO CS2 63x/1.20 water objective (Leica, Wetzlar, Germany) and Leica Application Suite X software (LASX, Leica, Wetzlar, Germany). The FITC emission signal was detected with a HyD (hybrid) detector in the range of 500–550 nm.

Ex vivo transdermal delivery studies

Transdermal insulin delivery was assessed by the Franz cell apparatus (Scheme 1; PermeGear, PA, USA). For preliminary evaluation, human skin (full thick) was obtained from Zenbio (NC, US). All other experiments were obtained from healthy women (between 30 and 65 years old) who were undergoing aesthetic abdominal surgery and had signed an informed consent form. The experiments were conducted with the approval of the IRB (Helsinki Committee) of Soroka Medical Center, Beer Sheva, Israel. A mechanical skin press apparatus was used to section the skin [with an average thickness of 2.2 ± 0.36 cm] and it was kept at -20 °C until it was used, but no more than three months to retain normal skin barrier.^{43,44} On the day of experiment, the skin samples were pre-equilibrated with the PBS for 1 h prior to use, with the dermal side submerged in the buffer. Then, the skin samples were clamped between the donor and receptor chambers, with the epidermal side facing the donor compartment (0.64 cm² diffusion areas and 5 mL receptor volumes were used). The donor chamber was loaded with 200 μL of the sunflower oil solutions of the biopolymers, all containing insulin (0.2 mg/mL). The sunflower oil containing insulin without biopolymer was used as a control treatment. The receptor chamber was filled with 5 mL of PBS containing sodium azide (prevent microbial growth) and kept at 37 ± 0.5 °C under constant stirring (500 rpm). Samples (200 μL each) were taken at the indicated time points and an equal volume of the buffer was added immediately.

To determine mass balance, the residual compounds in the donor chamber were collected, and five D-SQUAME® discs strips of the upper stratum corneum (nonspecific binding) were added and labeled as 'Donor'. Additional 15 tape strips were then taken to remove the stratum corneum and placed in glycine buffer supplemented with 0.5% Triton x-100 to elute the insulin. Then the epidermis and dermis were cut by a scalpel, submerged in glycine buffer supplemented with 0.5% Triton x-100 and vortex for 5 min to elute the insulin (labeled as 'viable skin').

The amount of insulin permeated was quantified by enzyme-linked immunosorbent assay (ELISA; Mercodia, Uppsala, Sweden), using a designated standard curve. All of the samples were tested in three repetitions.



Scheme 1. Efficacy experiments with a Franz diffusion cell apparatus image (PermeGear, PA, USA).

Skin integrity evaluation

Prior of the Franz cell permeation studies the skin samples integrity was visually evaluated. When indicated the following tests were also performed:

Trans Epidermal Water Loss (TEWL). Trans Epidermal Water Loss was measured before and after the application of the biopolymers to determine the initial integrity of the barrier and any change due to the compounds, respectively. Before applications, the epidermal side was dried to remove residual moisture from the buffer and hydration processes, and left for 20 min for equilibrium before TEWL measurement (The Multi Probe Adapter 6, Courage+Khazaka, Germany). After application, the compounds were removed, and the epidermal side was washed, dried with cotton applicators, and left for 20 min for equilibrium before TEWL measurement.

Methylene blue permeation test. Following exposure to the compound, the compounds were removed, and the epidermal side was washed, dried with cotton applicators and 100 μL of methylene blue solution (1% w/v) was added. After 30 min the receptor chamber was sampled, and colorimetric measurement was performed concomitantly with the generation of a standard curve. Increase in absorbance in comparison to the control was regarded as reduced barrier capacity of the skin.

Skin viability and irritation

All cell-culture media and reagents were purchased from Biological Industries (Beit-HaEmek, Israel). The skin samples were obtained from healthy women (between 30 and 65 years old) who were undergoing aesthetic abdominal surgery and had signed an informed consent form. The experiments were conducted with the approval of the IRB (Helsinki Committee) of Soroka Medical Center, Beer Sheva, Israel. Human skin culture preparation and treatments were performed under aseptic conditions. A mechanical skin-press apparatus was used to section the skin into 0.64-cm² pieces, as previously described (Scheme 2; left).⁴⁵ The skin explants were maintained in an air-liquid interface, with the dermal side submerged in the liquid. The biopolymers were applied topically (3 μL). After 48 h, the spent media was discarded and IL-1 α was evaluated by ELISA (Biolegend, CA, US). In addition, epidermis was separated and viability was determined by MTT, as previously reported after 48 h (Scheme 2; right).⁴⁶ For morphological evaluation, the samples were fixed with 4% formaldehyde for 1 h at room temperature. Then, the tissues were washed with PBS and kept in 70% ethanol at $2-8$ °C until use. Following dehydration, paraffin sections (10 μm) were prepared, and slides were stained with hematoxylineosin solution.



Scheme 2. Skin processing (left) and *ex vivo* safety measurements of human skin organ cultures (right).



Computational modelling

The 3D structures of cellulose 100mer chains were built using CarbBuilder program,⁴⁷ and 90 hydroxyls in D-glucose units were randomly substituted by carboxymethyl moieties (corresponding to DS 0.9) using our python program SubRandoMol.py and the Indigo library/modules.⁴⁸ Next, structures of CMC-6 and CMC-12 polymers were modelled by random replacement of CMC carboxy groups by 20 *N*-hexyl and 18 *N*-dodecyl-amide groups, according to our experimental DS values of 20% and 18% determined for CMC-6 and CMC-12, respectively.

Multiple molecular dynamics (MD) trajectories (10-50 ns) were generated for different single 100mer CMC-6 and CMC-12 polymer chains by GROMACS 2021.2⁴⁹ using the MD protocols.^{50,51} Different CMC-6 and CMC-12 single chains were placed into the 53×3.5×3.5 nm³ box filled by ~solvent (water) molecules. Total charges of CMC-6 (-78e) and CMC-12 (-72e) molecules were neutralized by 78 and 72 sodium (Na⁺) cations, respectively. Molecular topologies based on amber99SB and the carbohydrate GLYCAM06 force fields,⁵² were prepared for MD simulations using AmberTools and acpype programs.⁵³ For each trajectory, snapshots were collected, and the persistence length of CMC-6 and CMC-12 chains and conformational flexibility of CM groups and *N*-octyl-amide-CMC chains were analysed.

Results and discussion

Synthesis and characterization

The *N*-alkylamidated polysaccharides were synthesized in a one-step reaction of carboxymethyl cellulose (CMC) with hexylamine or dodecylamine to yield CMC-6 or CMC-12, respectively (Figure 1). The isolated products were characterized by ATR-FTIR and ¹H-NMR spectroscopy, which confirmed the successful coupling. The ATR-FTIR scans included new peaks for alkyl C-H bending at 680–720 cm⁻¹, amide frequencies at 1560–1580 cm⁻¹ and *N*-H stretch at ~3300 cm⁻¹. The ¹H-NMR scans showed the aliphatic protons of the coupled alkyl chains at 0.8–2.1 ppm and the α to amide bond protons at 2.8–3.2 ppm. The peaks of the original CMC were found to be in accordance with those reported in previous publications.⁵⁴ The new appearing peaks of the modified CMC-6 or CMC-12, correlate with FTIR^{55,56} and ¹H-NMR^{35,56} data of previously reported modified polysaccharides. Both characterizations methods verify the formation of new secondary amide bonds confirming *N*-alkylamide CMC modifications.

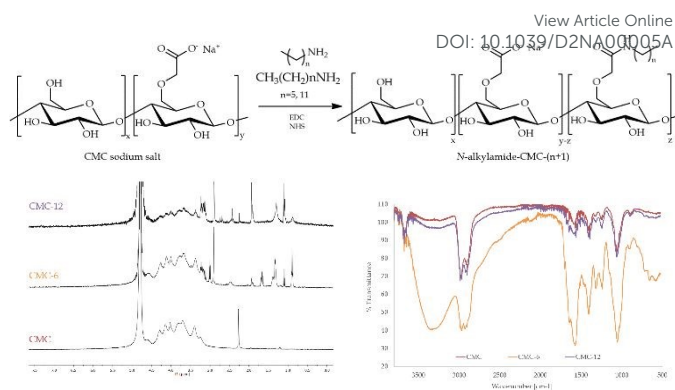


Figure 1. (Top) Synthesis of *N*-alkylamidated carboxymethyl cellulose derivatives, referred to as CMC-6 and CMC-12. ¹H-NMR 400 MHz (left) and ATR-FTIR (right) spectra of CMC and *N*-alkylamidated CMC-6 and CMC-12.

The modified polymers remain thermally stable. In TGA spectra, CMC-6 displayed a thermal decomposition pattern similar to that of the original CMC with a water weight loss event at ~ 57 °C and main pyrolytic decomposition events at 286.0 and 283.5 °C for CMC and CMC-6, respectively. The dodecyl substituted CMC-12 spectra was different, showing two defined pyrolytic decomposition events, one at 187.3 °C (with 20.3% weight loss) and the other at 290.0 (with 38.5% weight loss). The total weight loss for CMC, CMC-6, and CMC-12 were 77.6%, 71.9% and 87.2%, respectively. The water evaporation area points on ~ 10 % water content, which is expectable for polysaccharides. DSC studies showed thermal decomposition, without any prior glass transition because of semi-rigid nature of polysaccharide backbone (Figures 2 and S1).

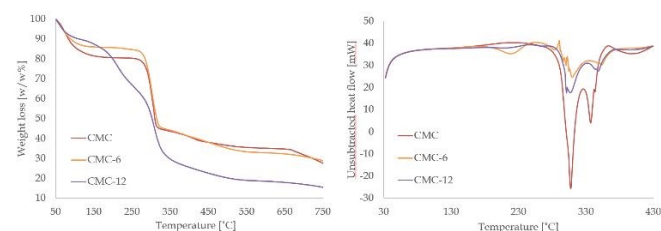


Figure 2. Thermal gravimetric analysis - TGA (left) and differential scanning calorimetry - DSC (right) for CMC, CMC-6 and CMC-12.

The degree of substitution was determined using the total organic carbon (TOC) method and was found to be 24% and 18% for CMC-6 and CMC-12, respectively. Conjugation with aliphatic amines provides the modified polysaccharides with amphiphilic properties, allowing spontaneous self-assembly that takes place above a specific concentration, termed the critical aggregation concentration (Table 1). Whereas the original CMC does not undergo self-assembly, CMC-6 and CMC-12 derivatives spontaneously assemble at concentrations above 1.66 and 0.05 mg/mL, respectively. Transmission electron microscopy (TEM) studies confirmed the formation of stable nanometric



aggregates, 50–150 nm in size for CMC-6 and 150–230 nm in size for CMC-12 (Figure 3).

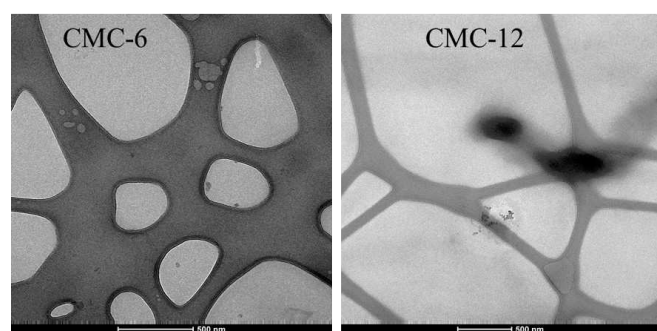


Figure 3. TEM images of CMC-6 (left) and CMC-12 (right). Scale bars are set to 500 nm.

Gel permeation chromatography (GPC) revealed that the coupled aliphatic chains caused a decrease in the retention time; the longer the chain, the shorter the retention time. The number average molecular weight (Mn) of the prepared polymers was calculated using dextran as a calibrating standard. Mn increases with the length of the coupled chain. It should, however, be noted that that Mn is better to be viewed as a comparing parameter and not as an absolute value, since spontaneous assembling ability affects gel permeation properties of the prepared CMC-6 and CMC-8, and their Mn values (Table 1).

Table 1. Physicochemical properties: degree of substitution (DS), critical aggregation concentration (CAC), retention time (RT), number average molecular weight (Mn) and polydispersity (PDI) for CMC, CMC-6 and CMC-12.

	DS [%]	CAC [mg/mL]	RT [min]	Mn [kDa]	PDI
CMC	-	-	10.397	154	1.97
CMC-6	24	1.66±0.58	9.486	584	2.95
CMC-12	18	0.05±0.004	8.653	5423	2.85

Transdermal delivery of insulin

First, *in vitro* studies of the abilities of CMC-6 and CMC-12 to introduce insulin into a lipid environment were performed. For this purpose, insulin labeled with the FITC fluorescent probe in sunflower oil was used. The encapsulation ability of the prepared systems was measured by spectrofluorimetry and confocal laser scanning microscopy (Figure 4). It can be seen that among all of the examined treatments, the CMC-12 nanocarrier demonstrated best performance.

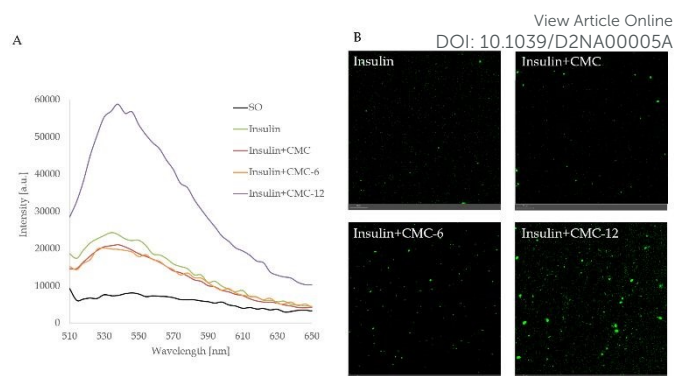


Figure 4. (A) Fluorescence emission spectra and (B) confocal laser scanning microscopy (CLSM) images of insulin labeled with fluorescein isothiocyanate dissolved in sunflower oil (SO) in the presence of CMC, CMC-6 and CMC-12. Scale bars are set to 20 μm .

At the next stage, the insulin carrying biopolymers were mounted on the Franz cell apparatus and the kinetics of their permeation across human skin was measured (infinite dose settings). As shown in Figure 5A, the unmodified CMC had no noticeable impact and did not enhance insulin permeation. While CMC-6 slightly enhanced insulin permeation, a massive increase was obtained using CMC-12 carrier, correlating with the results observed in *in vitro* studies. The superior performance of CMC-12 can be attributed to a long dodecyl substituent that increases the membrane penetration ability of that carrier. An effect of alkyl chain length on mass transport across membranes has been reported previously.⁵⁷ In addition, it can be speculated that dodecyl substituted CMC-12 biopolymer facilitates the formation of less tightly self-assembled structures, making it a better choice for the encapsulation of large macromolecules such as insulin. The fast kinetics shown here without a significant lag time is not characteristic for the permeation of macromolecules, such as insulin. However, Cevc *et al.* showed already in 1998 that carrier mediated transcutaneous insulin delivery by transferosomes can be rapid.⁵⁸ This was also true to the transdermal delivery of insulin by iodine facilitators.⁵⁹

In addition, the residual insulin in donor chamber was examined and a mirror image was seen (Figure 5b), given further supporting to the transdermal results. To further investigate the impact of the leading compound (CMC-12), a mass balance analysis was performed. The results shown in the lower panel of Figure 5 demonstrate the enhanced capacity of the biopolymers, less than 30% did not permeate through the stratum corneum.



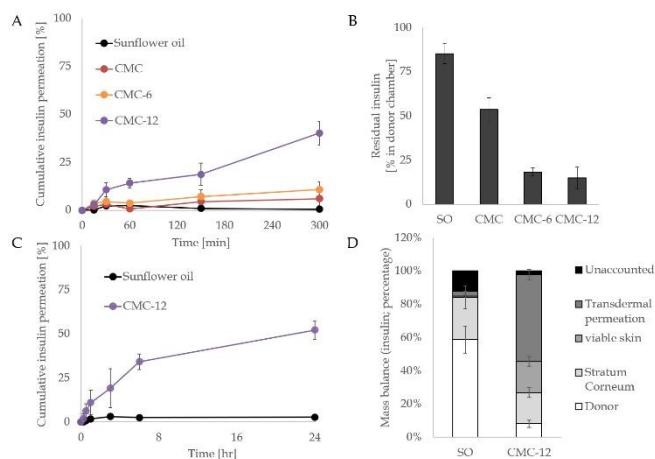


Figure 5. Transdermal experiments with a Franz diffusion cell apparatus. (A) Time-dependent permeation profile through human skin by periodic sampling. Insulin was quantified by ELISA, using a designated standard curve. (B) The residual insulin levels in the donor compartment are presented. (C) and (D) shows the complete analysis for CMC-12, the lead compound vs the control set (insulin in sunflower oil (SO)).

As fast kinetics was found together with high efficacy, the possibility that the barrier capacity of the skin was hampered by the biopolymers was addressed. For this purpose, two additional skin integrity tests were used, Trans Epidermal Water Loss (TEWL) and methylene blue permeation.^{60,61} In the following tests. The results shown in Table 2 depict the TEWL and methylene blue before the application of the compounds or after 5 or 24 hr. As can be seen, the initial readings were within the expected range. Importantly, water loss was not affected by the compound, which implies that the barrier function was unaltered by the different treatments. SDS treatment was used as a positive control that indeed increased water loss by almost 3-fold, confirming that this experimental setting enables to distinguish skin damage. Similarly, no detectable levels of methylene blue were found further demonstrating the integrity of the skin samples after exposure to the biopolymer-based delivery system.

To assess the potential of the biopolymer for efficient delivery of a precise dose, a second transdermal evaluation was tested, but with 5-fold lower insulin level (defined dose). As can be seen in Figure 6A, the system transferred above 85% of the insulin amount thought the dermal barrier. Thus, the biopolymers action can be controlled and foreseen after 1 hr of application.

Table 2. Trans Epidermal Water Loss (TEWL) test [$\text{g}/\text{m}^2/\text{hr}$] at 5 and 24 hrs post-Exposure (pE) and methylene blue permeation tests [$\mu\text{g}/\text{mL}$].

TEWL test	SO	CMC	CMC-6	CMC-12	SDS 10%
Baseline	9.6±0.79	9.3±0.63	8.1±0.38	9.7±0.19	10.0±2.4
pE 5 hr	10.1±2.7	9.2±0.67	7.0±1.76	9.1±1.70	27.1±3.3
Baseline	9.8±0.68	9.7±1.37	9.7±0.28	10.6±0.51	
pE 24 hr	10±0.45	10.1±0.33	10±0.22	9.7±0.76	
Methylene blue test					
		5 hr	24 hr		
SO		<0.01	<0.01		
CMC		<0.01	<0.01		
CMC-6		<0.01	<0.01		
CMC-12		<0.01	<0.01		
SDS 10 %		0.13±0.06			

Next, an *ex vivo* human skin organ culture was used to exclude the possibility of skin damage during the transdermal delivery process. The biopolymers were topically applied to the epidermal side of the skin. As expected, sodium dodecyl sulphate (SDS) markedly compromised skin viability, as seen in the MTT results (Figure 6B). However, none of the biopolymers had any negative effects on the skin, in comparison to the naïve untreated control (Figure 6C). Similar results were obtained from the histological evaluations: SDS markedly disrupted the epidermal layer; whereas no morphological alterations by the media (SO) or biopolymers were recorded. Lastly, the secreted level of the irritation cytokine IL-1 α ^{62,63} was used as an independent marker to assess the impact of the biopolymers on the skin. The results (Figure 6D) clearly showed no enhancement by the compounds. Thus, the biopolymers were verified to be both effective and safe. The results of TEWL and methylene blue tests combining with the skin irritation test shown in Figure 6, verify that the observed enhanced insulin penetration is highly unlikely the result of skin damage

To the best of our knowledge, polysaccharide-based systems for transdermal delivery of insulin have not been reported before. Synthetic polymers,³¹ fatty substances,³² ionic small molecules,³⁷ oily formulation,^{38,41} SAS,³⁹ and gold nanostructures-based^{40,41} systems were reported in this regard. Delivery systems based on polysaccharide benefit from biocompatibility, safety and cost-effectiveness, since nature sourced polysaccharides are widely available. The most important, the properties of such systems can be carefully tuned, since polysaccharides have well defined chemical structure of monomer units allowing predictable rationally modified.



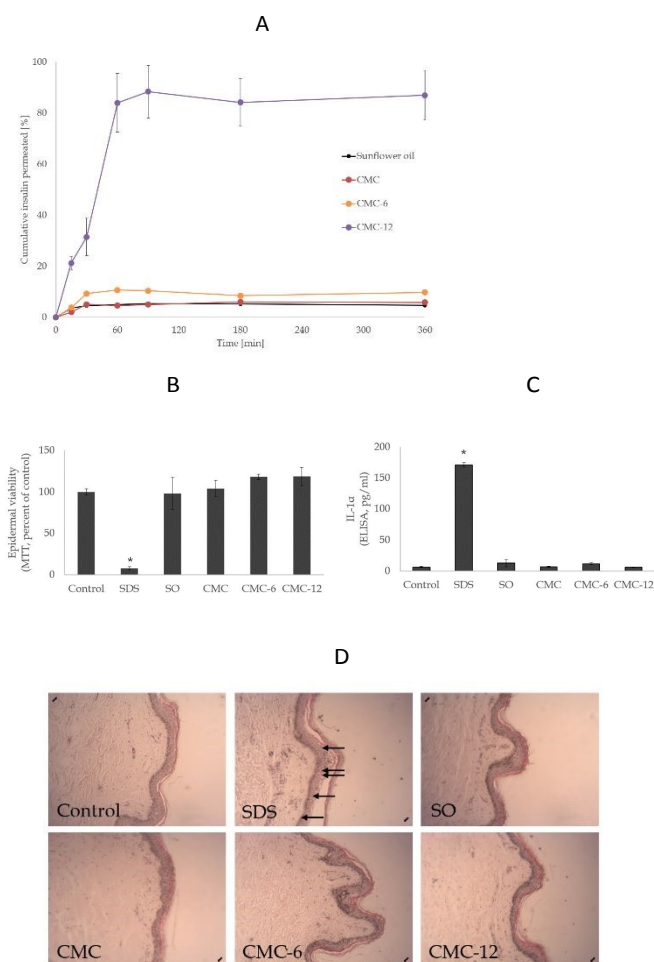


Figure 6. Efficacy and safety experiments in the ex vivo skin. (A) the time-dependent ability of the nanocapsules to transfer insulin across human skin was evaluated with a defined insulin content (55 μM). Insulin in sunflower oil (SO) was used as a control. (B) Epidermal viability experiments (MTT) as a percentage of the control. (C) Evaluation of cytokine IL-1 α by ELISA. (D) Histological evaluation of the morphology of the control and the topically treated human skin.

Three-dimensional molecular modelling

Three-dimensional molecular modelling and conformational dynamics studies of CMC-6 and CMC-12 in a dilute solution shows that almost all trajectories of both polymers are converged after 25–30 ns. The hydrophobic patches on the modified CMC surface created by *N*-alkyl groups can (1) interact with non-polar amino acids of insulin molecules, (2) contribute to self-aggregation of CMC molecules, and (3) transport the CMC-bound insulin into a lipid phase. According to our model, processes (2) and (3) are favoured by long *N*-alkyl chains and therefore are most pronounced for CMC-12.

Being solvated amphiphilic polymers that bear anionic carboxyl groups, CMC-6 and CMC-12 can be involved in the electrostatic interactions with cationic lysine (Lys) and arginine

(Arg) moieties. Indeed, significant charge complementarity between the positive charges on the molecular surfaces of insulin hexamer and the negative charges of CMC-based polysaccharides was found. Specifically, two arginine (Arg22) and two lysine (Lys29) moieties from two different subunits on the insulin hexamer surface are exposed to the bulk aqueous solution and therefore are accessible for electrostatic attraction to the carboxyl groups of the modified CMC polysaccharide (Figure 7 left). These attractions are possible due to clusters of 4–6 carboxyls on the polysaccharide surface that enhance the negative charge. These negatively charged clusters are attracted to the areas of the positive potential (blue) on the molecular surface of insulin (Figure 7 right).

Thus, in the *N*-alkylamidated CMC-based carriers the insulin binding is driven by electrostatic interactions, whereas the delivery into a lipid phase is promoted by long alkyl chains.

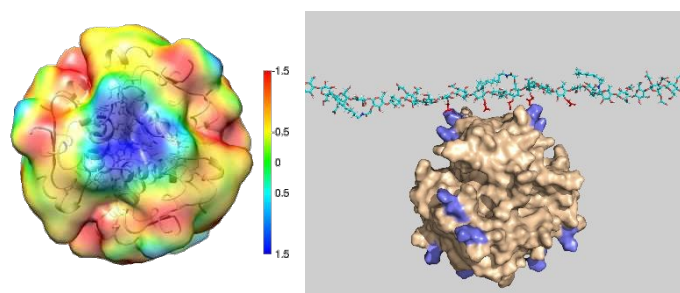


Figure 7. 3D modelling of the interaction between CMC-12 and the amino acid of the insulin (beige–insulin; lysine and arginine amino acids–purple; CMC polysaccharide–turquoise; carboxyl groups–red (left). 3D color map distribution represents the electrostatic potential on the surface of insulin; ranging from the negative (red, yellow) to the neutral and positive (green, blue) values (right).

Conclusions

This study demonstrates the successful achievement of a challenging goal: the transdermal delivery of hydrophilic macromolecules using biocompatible carriers without any auxiliary physical treatment. *N*-alkylamidated carboxymethyl cellulose polysaccharides, CMC-6 and CMC-12, capable of spontaneously assembling into soft nanocarriers were synthesized. These carriers exhibited a remarkable ability to self-adjust to aqueous and lipid environments and were, therefore, examined for transdermal delivery. The CMC-12 carrier led to a remarkable increase of transdermal delivery of insulin, showing a capacity of 85% of the compound in the receiver chamber. 3D molecular modelling and conformational dynamics studies shed light on the interactions of insulin molecules with the prepared carriers. Toxicity studies demonstrated high epidermal viability and the absence of cytokine release amplification, initially verifying their safety.

The presented materials have the potential to become a safe and feasible platform for effective transdermal delivery of bioactive macromolecules in medicine and cosmetics. The progress in transdermal delivery of insulin is of particular importance, however additional studies are of need. Additional



challenges need to be addressed prior to clinical usages of this new delivery system. The permeated insulin levels should be precisely regulated to reduce the possibility of hypo- or hyperglycemia. The topical formulation and application area should also be controlled. The integration of insulin-containing carriers into a transdermal patch, for instance, will provide an easy way to control both the dosage and the surface area. In addition, in vivo validation of safety (multiple dosage) and efficacy need to be done in the further studies.

Author Contributions

Conceptualization, Y.C. E.F. and E.P.; Methodology, Y.C., G.C. and D.T.; Software, Y.C. and D.T.; Validation, Y.C. and E.P.; Formal Analysis, Y.C. and G.C.; Investigation, Y.C. and N.E.K.; Resources, G.C., E.S., E.F. and E.P.; Writing – Original Draft Preparation, Y.C.; Writing – Review & Editing, Y.C., G.C., D.T., E.S. and E.P.; Visualization, Y.C. and E.P.; Supervision, G.C., E.F. and E.P.; Project Administration, Y.C. and E.P.; Funding Acquisition, G.C. and E.P.

Conflicts of interest

The authors declare no conflict of interest.

Acknowledgements

The authors would like to thank Dr. Yael Levi-Kalisman for providing technical support for the TEM imaging, Eduard Belausov for his help with CLSM and Raanan Gvirts for his help with the Franz cell apparatus. G.C. is partially supported by the Israel Ministry of Science and Technology (580458776).

Notes and references

- 1 R. Yang, T. Wei, H. Goldberg, W. Wang, K. Cullion and D. S. Kohane, *Adv. Mater.*, 2017, **29**, 1606596.
- 2 M. J. Webber, E. A. Appel, E. W. Meijer and R. Langer, *Nat. Mater.*, 2015, **15**, 13–26.
- 3 J. Kim, D. Jang, H. Park, S. Jung, D. H. Kim and W. J. Kim, *Adv. Mater.*, 2018, **30**, 1707351.
- 4 Y. Cao and R. Mezzenga, *Nat. Food*, 2020, **1**, 106–118.
- 5 W. F. Lai and H. C. Shum, *ACS Appl. Mater. Interfaces*, 2015, **7**, 10501–10510.
- 6 D. Witzigmann, D. Wu, S. H. Schenk, V. Balasubramanian, W. Meier and J. Huwyler, *ACS Appl. Mater. Interfaces*, 2015, **7**, 10446–10456.
- 7 E. M. Bachelder, E. N. Pino and K. M. Ainslie, *Chem. Rev.*, 2017, **117**, 1915–1926.
- 8 B. Ates, S. Koytepe, A. Ulu, C. Gurses and V. K. Thakur, *Chem. Rev.*, 2020.
- 9 Y.-H. Zhang, Y.-M. Zhang, J. Yu, J. Wang and Y. Liu, *Chem. Commun.*, 2019, **55**, 1164–1167.
- 10 R. Malviya, P. K. Sharma and S. K. Dubey, *Mater. Sci. Eng. C*, 2016, **68**, 929–938.

- 11 V. G. Muir and J. A. Burdick, *Chem. Rev.*, 2021.
- 12 M. Grossutti and J. R. Dutcher, *Biomacromolecules*, 2020, **21**, 4871–4877.
- 13 Y. Cohen, R. Rutenberg, G. Cohen, B. Veltman, R. Gvirts, E. Fallik, D. Danino, E. Eltzov and E. Poverenov, *ACS Appl. Bio Mater.*, 2020, **3**, 2209–2217.
- 14 M. R. Prausnitz and R. Langer, *Nat. Biotechnol.*, 2008, **26**, 1261–1268.
- 15 M. S. Kapoor, A. D'Souza, N. Aibani, S. S. Nair, P. Sandbhor, D. Kumari and R. Banerjee, *Sci. Rep.*, 2018, **8**, 16122.
- 16 X. H. Wang, T. Su, J. Zhao, Z. Wu, D. Wang, W. N. Zhang, Q. X. Wu and Y. Chen, *Cellulose*, 2020, **27**, 10277–10292.
- 17 J. Laubach, M. Joseph, T. Brenza, V. Gadhamshetty and R. K. Sani, *J. Control. Release*, 2020.
- 18 Kalave S, Chatterjee B, Shah P, Misra A. *Curr Pharm Des.* 2021, **27**, 4330-4340. DOI: 10.2174/1381612827666210820095330. PMID: 34414868.
- 19 J. D. Bos and M. M. H. M. Meinardi, *Exp. Dermatol.*, 2000, **9**, 165–169.
- 19 Y. Zhang, J. Yu, A. R. Kahkoska, J. Wang, J. B. Buse and Z. Gu, *Adv. Drug Deliv. Rev.*, 2019, **139**, 51–70.
- 20 E. S. Khafagy, M. Morishita, Y. Onuki and K. Takayama, *Adv. Drug Deliv. Rev.*, 2007, **59**, 1521–1546.
- 21 R. Bilous and R. Donnelly, *Handbook of Diabetes*, 4th edn., 2010.
- 22 J. Cao, N. Zhang, Z. Wang, J. Su, J. Yang, J. Han and Y. Zhao, *Pharmaceutics*, 2019, **11**, 235.
- 23 S. Liu, M. N. Jin, Y. S. Quan, F. Kamiyama, K. Kusamori, H. Katsumi, T. Sakane and A. Yamamoto, *Eur. J. Pharm. Biopharm.*, 2014, **86**, 267–276.
- 24 I.-C. Lee, W.-M. Lin, J.-C. Shu, S.-W. Tsai, C.-H. Chen and M.-T. Tsai, *J. Biomed. Mater. Res. Part A*, 2017, **105**, 84–93.
- 25 B. Xu, G. Jiang, W. Yu, D. Liu, Y. Zhang, J. Zhou, S. Sun and Y. Liu, *J. Mater. Chem. B*, 2017, **5**, 8200–8208.
- 26 P. Zhang, Y. Zhang and C. G. Liu, *RSC Adv.*, 2020, **10**, 24319–24329.
- 27 S. Lee, B. Snyder, R. E. Newnham and N. Barrie Smith, *Diabetes Technol. Ther.*, 2004, **6**, 808–815.
- 28 J. Elisseeff, K. Anseth, D. Sims, W. Mcintosh, M. Randolph and R. Langer, *Proc. Natl. Acad. Sci. U. S. A.*, 1999, **96**, 3104–3107.
- 29 C. Lombry, N. Dujardin and V. Pr eat, *Pharm. Res.*, 2000, **17**, 32–37.
- 30 A. Sen, M. E. Daly and S. W. Hui, *Biochim. Biophys. Acta - Biomembr.*, 2002, **1564**, 5–8.
- 31 Y. Chen, Y. Shen, X. Guo, C. Zhang, W. Yang, M. Ma, S. Liu, M. Zhang and L. P. Wen, *Nat. Biotechnol.*, 2006, **24**, 455–460.
- 32 J. Guo, Q. Ping and L. Zhang, *Drug Deliv. J. Deliv. Target. Ther. Agents*, 2000, **7**, 113–116.
- 33 B. Godin and E. Touitou, *Crit. Rev. Ther. Drug Carrier Syst.*, 2003, **20**, 63–102.
- 34 M. Witting, A. Boreham, R. Brodewolf, K. Vavrova, U. Alexiev, W. Friess and S. Hedtrich, *Mol. Pharm.*, 2015, **12**, 1391–1401.
- 35 S. Son, J. Lim, T. Kang, J. Jung and E.-K. Lim, *Nanomaterials*, 2017, **7**, 427.



- 36 S. Zhang, P. Xin, Q. Ou, G. Hollett, Z. Gu and J. Wu, *J. Mater. Chem. B*, 2018, **6**, 6723–6730.
- 37 E. E. L. Tanner, K. N. Ibsen and S. Mitragotri, *J. Control. Release*, 2018, **286**, 137–144.
- 38 Y. Tahara, S. Honda, N. Kamiya and M. Goto, *Medchemcomm*, 2012, **3**, 1496–1499.
- 39 X. Zhao, Y. Zu, S. Zu, D. Wang, Y. Zhang and B. Zu, <http://dx.doi.org/10.3109/03639041003695089>, 2010, **36**, 1177–1185.
- 40 M. Shilo, P. Berenstein, T. Dreifuss, Y. Nash, G. Goldsmith, G. Kazimirsky, M. Motiei, D. Frenkel, C. Brodie and R. Popovtzer, *Nanoscale*, 2015, **7**, 20489–20496.
- 41 K. Nose, D. Pissuwan, M. Goto, Y. Katayama and T. Niidome, *Nanoscale*, 2012, **4**, 3776–3780.
- 42 O. Setter and Y. D. Livney, *Phys. Chem. Chem. Phys.*, 2015, **17**, 3599–3606.
- 43 T. S. Pereira, G. N. Gotor, L. S. Beltrami, C. G. Nolla, J. A. V. Rocha, F. P. Broto, L. R. Comellas and V. M. F. Vargas, *Mutat. Res. - Genet. Toxicol. Environ. Mutagen.*, 2010, **702**, 78–85.
- 44 I. Kielhorn, J., Melching-Kollmuss, S., Mangelsdorf, *IPCS: Dermal Absorption; Environmental health criteria; 235; Geneva*, Hanover, Germany, 2006.
- 45 N. Ogen-Shtern, K. Chumin, G. Cohen and G. Borkow, *J. Cosmet. Dermatol.*, 2020, **19**, 1522–1527.
- 46 S. Kahremany, I. Babaev, R. Gvirtz, N. Ogen-Stern, S. Azoulay-Ginsburg, H. Senderowitz, G. Cohen and A. Gruzman, *Skin Pharmacol. Physiol.*, 2019, **32**, 173–181.
- 47 M. M. Kuttel, J. Stähle and G. Widmalm, *J. Comput. Chem.*, 2016, **37**, 2098–2105.
- 48 M. Pavlov, D.; Rybalkin, Indigo Toolkit, <https://lifescience.opensource.epam.com/indigo/index.html>, (accessed 12 November 2021).
- 49 Welcome to the GROMACS documentation! — GROMACS 2021.2 documentation, <https://manual.gromacs.org/documentation/2021.2/index.html>, (accessed 23 November 2021).
- 50 Y. Yu, T. Tyrikos-Ergas, Y. Zhu, G. Fittolani, V. Bordoni, A. Singhal, R. J. Fair, A. Grafmüller, P. H. Seeberger and M. Delbianco, *Angew. Chem. Int. Ed. Engl.*, 2019, **58**, 13127–13132.
- 51 Y. Tidhar, H. Weissman, D. Tworowski and B. Rybtchinski, *Chem. - A Eur. J.*, 2014, **20**, 10332–10342.
- 52 K. N. Kirschner, A. B. Yongye, S. M. Tschampel, J. González-Outeiriño, C. R. Daniels, B. L. Foley and R. J. Woods, *J. Comput. Chem.*, 2008, **29**, 622–655.
- 53 A. W. Sousa Da Silva and W. F. Vranken, *BMC Res. Notes*, , DOI:10.1186/1756-0500-5-367.
- 54 H. Kono, K. Oshima, H. Hashimoto, Y. Shimizu and K. Tajima, *Carbohydr. Polym.*, 2016, **146**, 1–9.
- 55 T. Taubner, A. Synytsya and J. Čopíková, *Int. J. Biol. Macromol.*, 2015, **72**, 11–18.
- 56 A. Pettignano, A. Charlot and E. Fleury, *Polym. 2019, Vol. 11, Page 1227*, 2019, **11**, 1227.
- 57 G. L. Flynn and S. H. Yalkowsky, *J. Pharm. Sci.*, 1972, **61**, 838–852.
- 58 G. Cevc, D. Gebauer, J. Stieber, A. Schätzlein and G. Blume, *Biochim. Biophys. Acta - Biomembr.*, 1998, **1368**, 201–215.
- 59 A. C. Sintov and U. Wormser, *J. Control. Release*, 2007, **115**, 185–188.
- 60 K. Guth, M. Schäfer-Korting, E. Fabian, R. Landsiedel and B. van Ravenzwaay, *Toxicol. Vitro.*, 2015, **29**, 113–123.
- 61 F. K. Akomeah, G. P. Martin and M. B. Brown, *J. Pharm. Sci.*, 2007, **96**, 824–834.
- 62 R. Gvirtz, N. Ogen-Shtern and G. Cohen, *Pharmaceutics*, 2020, **12**, 299.
- 63 D. S. Olsen, M. Lee and A. P. Turley, *Toxicol. Vitro.*, 2018, **50**, 426–432.

